High spin states in ^{93}Tc

S. S. Ghugre, S. B. Patel, and M. Gupta
Departement of Physics, University of Bombay, Vidyanagari, Bombay 400 098, India

R. K. Bhowmik
Nuclear Science Centre, New Delhi 110 067, India

J. A. Sheikh
Tata Institute of Fundamental Research, Bombay 400 005, India
(Received 2 September 1992)

High spin states in the $N=50$ nucleus ^{93}Tc were populated and studied using the reaction ^{66}Zn (^{31}P, $2p2n$)^{93}Tc at a beam energy of 115 MeV. Gamma ray intensities and gamma-gamma coincidences were measured. Multipolarities of the transitions were extracted assuming stretched transitions. The positive and negative parity bands have been extended up to spins $\frac{39}{2}^+$ and $\frac{43}{2}^-$, respectively. The proposed level scheme above $J=\frac{25}{2}$ cannot be well understood on the basis of the spherical shell model calculations with valence protons occupying the $(1f_{5/2},2p_{3/2},2p_{1/2},1g_{9/2})$ configuration space. The breaking of the $N=50$ neutron core appears to be a plausible mechanism for the observed high spin states.

PACS number(s): 23.20.Lv, 23.20.En, 21.60.Cs, 27.60.+j

I. INTRODUCTION

It is well recognized [1,2] that the low-lying states in $N=50$ nuclei, for example, ^{89}Y, ^{90}Zr, ^{91}Nb, ^{92}Mo, ^{93}Tc, can be described with the valence protons occupying the $(2p_{1/2},1g_{9/2})$ configuration with ^{88}Sr as the closed core. However, with the advent of the Compton suppressed gamma detector arrays the level schemes of some of the $N=50$ nuclei have been extended to higher spin regimes. The shell-model configuration space needs to be enlarged to account for these observed high spin states. In a recent work [3,4], a larger configuration space $(1f_{5/2},2p_{3/2},2p_{1/2},1g_{9/2})$ for the valence protons has been employed in the shell-model calculations. Another possible mechanism to generate the higher angular momentum states is to break the $N=50$ closed shell. The high spin states observed in ^{94}Ru (Ref. [5]) have been described with the breaking of this neutron closed core. It is therefore of interest to study the high spin states in the $N=50$ nuclei systematically in order to explore the possible mechanism for generating these states.

Furthermore, an interesting experimental result for Sn isotopes with $Z=50$ (Refs. [6–8]) was the observation of deformed bands at higher excitation energies. A cascade of quadrupole transitions was observed in these Sn nuclei suggesting a collective behavior. The moment of inertia was found to be almost constant at high spins implying good rotor behavior. This surprising aspect in conjunction with a desire to systematically explore the possible mechanism for the high spin states, has motivated us to investigate $N=50$ nuclei, which although spherical in the low spin region may show some collectivity at high spins. In the present paper we report our study of the nucleus ^{93}Tc.

We have investigated high spin states in ^{93}Tc using the ^{66}Zn(^{31}P,$2p2n$)^{93}Tc reaction. In the previous work [9,10] the positive and negative parity bands in ^{93}Tc were investigated upto spins of $\frac{25}{2}^+$ and $\frac{25}{2}^-$, respectively. Using the above heavy ion reaction in conjunction with an array of six Compton suppressed Ge detectors, we have extended the level scheme of ^{93}Tc substantially. The negative parity band has been extended upto spin state of $\frac{43}{2}^-$ whereas the positive parity band now goes upto a spin state of $\frac{39}{2}^+$.

II. EXPERIMENTAL DETAILS AND ANALYSIS

High spin states in ^{93}Tc were populated using the ^{66}Zn($^{31}P,2p2n$)^{93}Tc reaction at a beam energy of 115 MeV. The ^{31}P beam was provided by the 15 UD Pelletron Accelerator at the Nuclear Science Centre (NSC), New Delhi. The relative production cross sections of the residues in the above reaction were consistent with those predicted by the statistical model code CASCADE. The isotopically enriched (99%)^{66}Zn target had a thickness of about 1.2 mg cm^{-2} and a 20 mg cm^{-2} Pb backing. Gamma-gamma coincidences were measured using the gamma detector array (GDA) at the NSC.

At the time of these measurements the GDA consisted of six Compton suppressed germanium detectors and a fourteen element bismuth germanate (BGO) multiplicity filter. The anti-Compton shields (ACS) of symmetric design were made of BGO with NaI caps in the front. The germanium detectors used were 23% n-type high-purity germanium (HPGe). The HPGe detectors were mounted inside the ACS such that the distance between the target and the Ge crystal face was 180 mm. Heavymet (tantalum alloy) collimators of thickness 30 mm each were set between each detector and the target to prevent any direct radiation from the target on the ACS.

The Compton suppressed HPGe detectors were incorporated in the mechanical structure in two groups of

three detectors each, in an out-of-plane arrangement shown in Fig. 1, for two detectors. One such group corresponded with an angle of 99° with the beam direction, while the other group corresponded with an angle of 153° with the beam direction. A Compton suppressed Ge detector gave typically a peak-to-total ratio of about 55% for the ^{60}Co gamma rays.

A BGO castle consisting of seven 38 mm×75 mm hexagonal elements was mounted above and below the scattering chamber at a distance of 40 mm from the reaction plane. The multiplicity filter covered only about 35% of the total solid angle. Due to this we have not used the multiplicity information for our analysis.

The on line data acquisition system was configured using the Micro-Vax computer connected to the CAMAC (a standardized multiplexing intermediate interface) through the Q-bus compatible KS 2922 interface card. It was possible to support up to 8 serial CAMAC crates, connected via a 40 wire ribbon cable with direct memory access (DMA) capability of 250 kilowords.

The multiparameter data was saved block by block onto the magnetic tapes, with a maximum block size of 16 384 bytes. The list mode data contained a pattern word identifying the detectors in coincidence, the energies of the corresponding gamma rays and additional information such as multiplicity. Our criteria for taking data onto the magnetic tapes corresponded to twofold or higher-fold coincidences. Thus corresponding to the master gate mainly two of the detectors would contain nonzero data. Clearly it was desirable to avoid writing these zeros onto the magnetic tapes. A ZERO-SUPPRESSION algorithm has been incorporated in the software by encoding a pattern word from the nonzero analog-to-digital converters (ADCs). This has prevented any data originating from false triggering due to the noise from getting written on the magnetic tapes and has resulted in a saving of the magnetic tapes used by a factor of about 3.

The ^{93}Tc gamma rays have been placed in the level scheme using the observed coincidence relationship and the intensity argument for gamma rays. The typical gamma coincidence rate was 150 counts per second and 25×10^6 events corresponding to a twofold or higher-fold coincidences (within a system timing resolution of 40 ns) were recorded in list mode.

The pulse height in each detector were software gain matched and the data was sorted out into a 1024×1024 total E_γ-E_γ matrix. From the processed data background subtracted one-dimensional histograms for gamma energies in one detector gated by a suitable transition in the other detector could be generated.

In order to assign multipolarities to the observed gamma transitions the data was sorted out into another two-dimensional array (1024×1024), such that the events recorded in the three detectors at 99° with respect to the beam direction were plotted along the y axis (after appropriate software gain matching to 1 keV per channel). The data from the other group of detectors at 153° with respect to the beam direction were then plotted along the x axis. Following the procedure given in Ref. [11] a gate corresponding to a gamma ray of known multipolarity is taken for the detectors on x axis and the gamma-ray spectrum for detectors along y axis is projected through it. Next the same gate is taken for the y axis detectors and gamma spectrum for detectors along the x axis is projected through it. Assuming the commonly encountered stretched transitions ($E2$ and $M1$), the intensities of those gamma rays which have the same multipolarity as the gated ray will be equal in the two projected spectra. On the other hand, the intensities differ by a factor of about 2 in the two projections, if the multipolarities of the projected gamma rays are different. Figure 2 shows the result of such a procedure. For the 1095 keV gate, the two projections result in the same intensity for the 607 keV gamma ray indicating that this is an $E2$ transition. Earlier studies [9,10] have shown that both the 1095 and 607 keV transitions are $E2$ in character. On the other hand, the intensities of most of the other

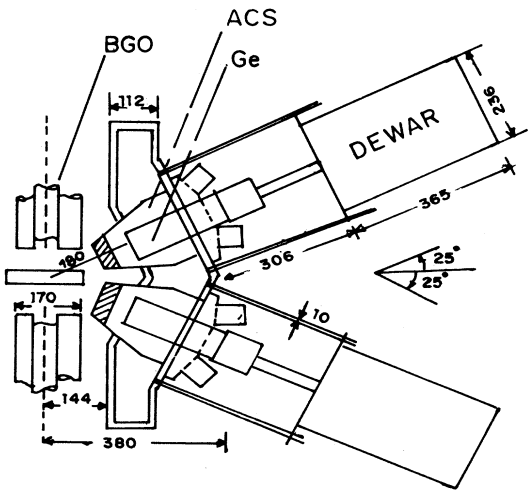

FIG. 1. Drawing shows two of the GDA detectors.

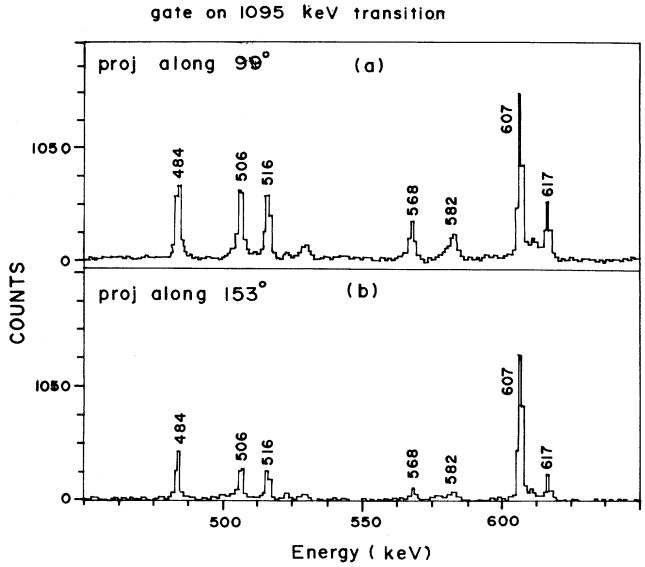

FIG. 2. Projections along the (a) 99° (b) 153° of the γ-γ coincidence spectra with gate on 1095 keV ($\frac{21}{2}^- \rightarrow \frac{17}{2}^-$) transition.

members of the band change by a factor of about 2 in the two projections implying that they are $M1$ in character.

III. EXPERIMENTAL RESULTS

Figures 3(a) and 3(b) show the spectra that were in coincidence with the 1434 keV ($\frac{3}{2}^+ \rightarrow \frac{9}{2}^+$) and the 1095 keV ($\frac{21}{2}^- \rightarrow \frac{17}{2}^-$) transitions in the positive and negative parity bands, respectively, for ^{93}Tc. The new gamma rays observed in the negative parity band were 484 keV ($M1$), 516 keV ($M1$), 506 keV ($M1$), 617 keV ($M1$), 355 keV ($M1$), 568 keV ($M1$), 320 keV ($M1$), 923 keV ($E2$), 1000 keV ($E2$), 1022 keV ($E2$), and 607 keV ($E2$). These transitions were placed above the $\frac{25}{2}^-$ level in the negative parity band. The multipolarity assignment was based on the procedure described in the previous section. We are reasonably certain about the position of these new gamma rays in the level scheme. We have gated on all the gamma rays and looked at the intensity flow above and below the gated gamma ray. The positioning of the gamma rays in the level scheme was consistent with this intensity flow pattern. Table I gives the excitation energy (E_x), transition energy (E_γ), the relative intensity (I_γ),

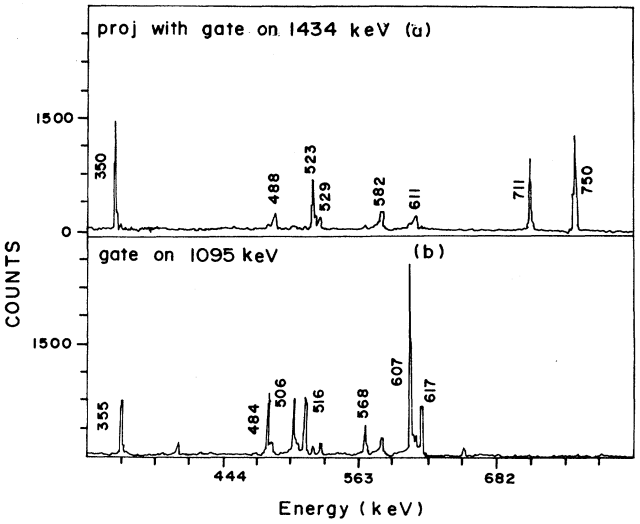

FIG. 3. (a) Part of the γ-γ coincidence spectrum for ^{93}Tc with gate on the gamma transition 1434 keV ($\frac{13}{2}^+ \rightarrow \frac{9}{2}^+$). (b) Part of the γ-γ coincidence spectrum for ^{93}Tc with gate on the gamma transition 1095 keV ($\frac{21}{2}^- \rightarrow \frac{17}{2}^-$).

TABLE I. Excitation energies (E_x), transition energy (E_γ), relative intensity (I_γ), and spin states in ^{93}Tc.

E_x (keV)	E_γ (keV)	I_γ	$J_i \rightarrow J_f$
1434.1	1434.1	100.0(3)	$\frac{13}{2}^+ \rightarrow \frac{9}{2}^+$
2184.2	750.1	57.3(4)	$\frac{17}{2}^+ \rightarrow \frac{13}{2}^+$
2534.0	349.8	26.3(5)	$\frac{21}{2}^+ \rightarrow \frac{17}{2}^+$
4256.4	1722.4	18.5(7)	$\frac{25}{2}^+ \rightarrow \frac{21}{2}^+$
4779.3	522.9	22.0(5)	$\frac{29}{2}^+ \rightarrow \frac{25}{2}^+$
6085.0	1306.1	12.5(10)	$\frac{33}{2}^+ \rightarrow \frac{29}{2}^+$
5267.1	487.8	5.1(12)	$\frac{31}{2}^+ \rightarrow \frac{29}{2}^+$
6085.0	817.9	8.7(8)	$\frac{33}{2}^+ \rightarrow \frac{31}{2}^+$
6667.5	582.5	7.9(8)	$\frac{35}{2}^+ \rightarrow \frac{33}{2}^+$
7278.8	611.3	4.9(14)	$\frac{37}{2}^+ \rightarrow \frac{35}{2}^+$
7808.3	529.5	3.7(12)	$\frac{39}{2}^+ \rightarrow \frac{37}{2}^+$
3310.2	1095.2	a	$\frac{21}{2}^- \rightarrow \frac{17}{2}^-$
3917.5	607.3	59.6(4)[b]	$\frac{25}{2}^- \rightarrow \frac{21}{2}^-$
7570.4	607.3		$\frac{41}{2}^- \rightarrow \frac{37}{2}^-$
4917.1	1000.1	(w)[e]	$\frac{29}{2}^- \rightarrow \frac{25}{2}^-$
4401.4	483.9	19.2(6)	$\frac{27}{2}^- \rightarrow \frac{25}{2}^-$
4917.1	515.7	c	$\frac{29}{2}^- \rightarrow \frac{27}{2}^-$
5423.5	1022.4	w[e]	$\frac{31}{2}^- \rightarrow \frac{27}{2}^-$
5423.5	506.4	d	$\frac{31}{2}^- \rightarrow \frac{29}{2}^-$
6040.6	617.1	24.6(5)	$\frac{33}{2}^- \rightarrow \frac{31}{2}^-$
6963.1	922.6	(w)[e]	$\frac{37}{2}^- \rightarrow \frac{33}{2}^-$
6395.2	354.6	5.1(7)	$\frac{35}{2}^- \rightarrow \frac{33}{2}^-$
6963.1	567.9	10.5(10)	$\frac{37}{2}^- \rightarrow \frac{35}{2}^-$
7890.1	319.7	1.6(11)	$\frac{43}{2}^- \rightarrow \frac{41}{2}^-$

[a] Intensity could not be computed as there exists another identical transition in ^{92}Mo.
[b] I_γ includes both 607 keV transitions.
[c] Intensity could not be computed as there exists another identical transition in ^{94}Tc.
[d] Intensity could not be computed due to the presence of the 511 keV annihilation photon.
[e] (w) refers to the weak crossover transitions mentioned in the text.

and the spin assignment of the gamma rays. All the intensities were efficiency corrected.

Several cross transitions were observed in the negative parity band. These were found to be $E2$ in character with energies of 1000, 1022, and 923 keV. A gate on these weak gamma rays reveal all other members of the negative parity band except the two $M1$ transitions (one of which originates from the same level) which run parallel to it and whose energies add up to give the energy of the gated $E2$ transition.

A gate on the 1000 keV ($\frac{29}{2}^- \rightarrow \frac{25}{2}^-$) gamma ray showed all members of the negative parity band except the two gamma rays 516 keV ($\frac{29}{2}^- \rightarrow \frac{27}{2}^-$) and 484 keV ($\frac{27}{2}^- \rightarrow \frac{25}{2}^-$). Similarly a gate on either the 484 or 516 keV showed that the 1000 keV gamma ray is not in coincidence with them while other members are. This is shown in Fig. 4. A similar situation was observed in case of the weak $E2$ transitions of energies 1022 and 923 keV. The existence of these cross transitions makes the proposed level scheme very likely; the depopulation pattern gets tied down.

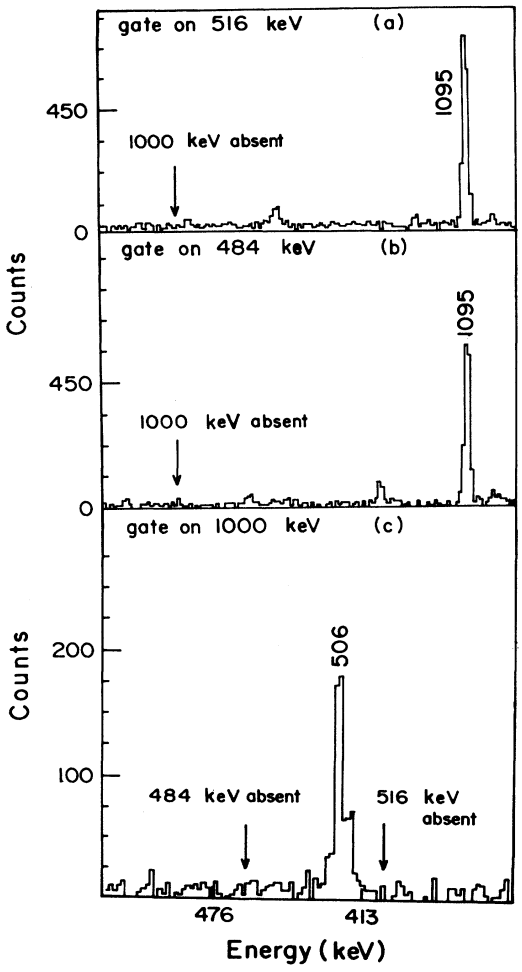

FIG. 4. (a),(b) Partial γ-γ coincidence spectra with gate on 516 ($\frac{29}{2}^- \rightarrow \frac{27}{2}^-$) and 484 ($\frac{27}{2}^- \rightarrow \frac{25}{2}^-$) keV transitions. The 1000 keV transition is absent. (c) Partial γ-γ coincidence spectrum with gate on 1000 keV ($\frac{29}{2}^- \rightarrow \frac{25}{2}^-$) transition. 484 and 516 keV transitions are absent.

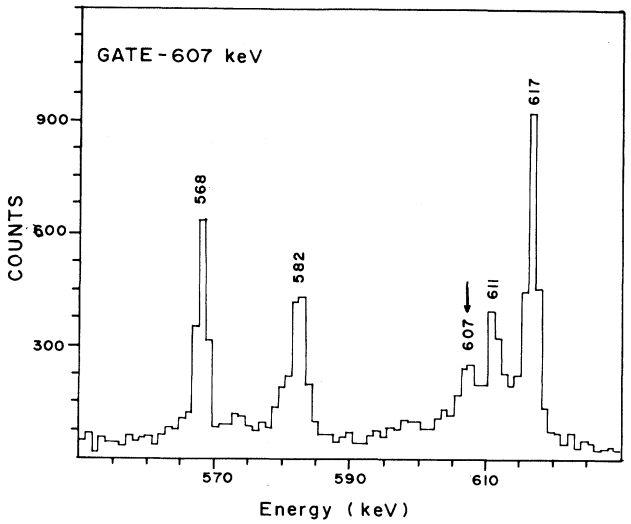

FIG. 5. Partial γ-γ coincidence spectrum with gate on 607 keV transition. The presence of another 607 keV γ ray indicates that the 607 keV γ ray is in coincidence with itself.

An interesting observation was that the 607 keV gamma ray was in coincidence with itself. Figure 5 shows this gated spectrum. This implies that there were two gamma rays of the same energy of 607 keV. Using intensity argument we have placed the second 607 keV gamma

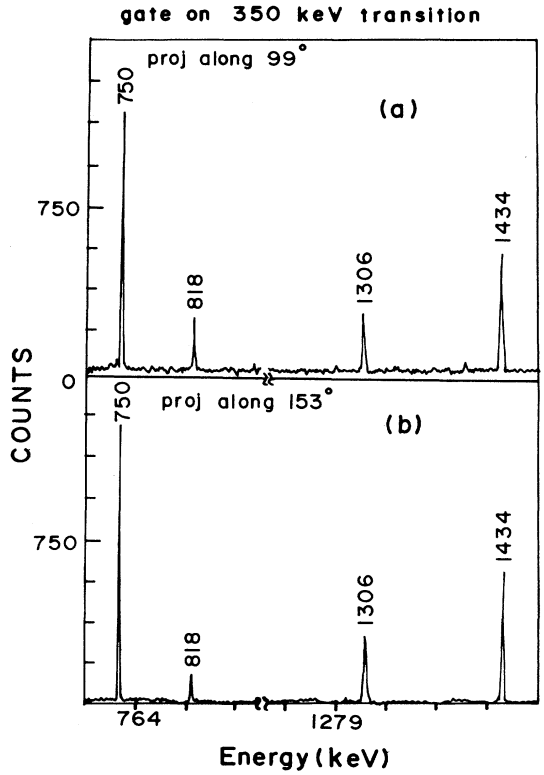

FIG. 6. Projections along the (a) 99° and (b) 153° of the γ-γ coincidence spectra with gate on 350 keV ($\frac{21}{2}^+ \rightarrow \frac{17}{2}^+$) transition.

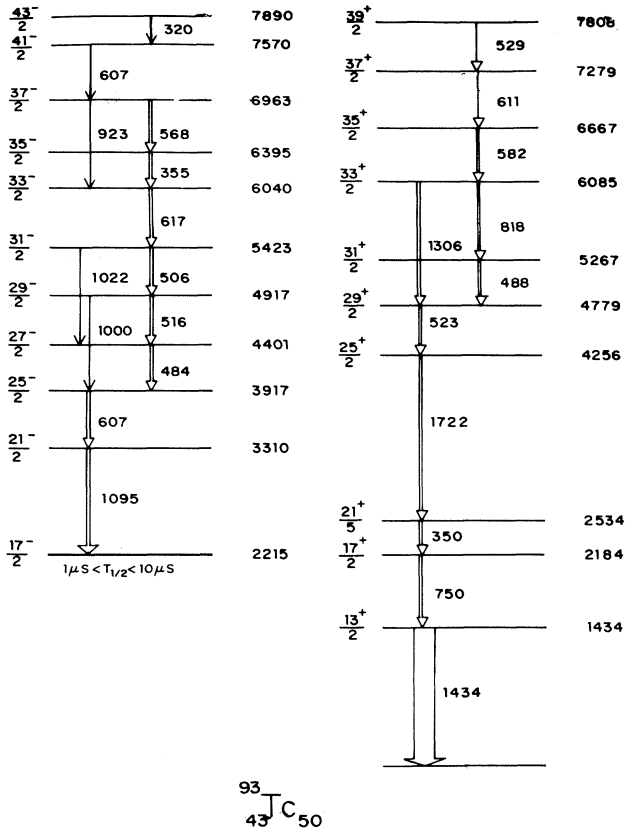

FIG. 7. Level scheme for ^{93}Tc showing excitation and gamma transition energies (in keV) for the levels populated in ^{66}Zn(^{31}P,2p2n)^{93}Tc reaction. Only levels above the $\frac{17}{2}^-$ isomeric state in the negative parity band are shown. The γ intensities are approximately equal to the width of the arrows.

ray near the top of the negative parity band.

In addition to the new transitions mentioned above a 402 keV $E2$ gamma ray was observed in coincidence with all other members of the negative parity band except the 484 and 320 keV transitions. We have not been able to place this transition in the decay scheme. Another observation which has not been understood is the occurrence of the 582, 611, and 529 keV transitions in coincidence with some transitions in the negative parity band.

The positive parity band was extended upto a spin of $\frac{39}{2}^+$. The new gamma rays observed were 488 keV ($M1$), 818 keV ($M1$), 582 keV ($E2$), 592 keV ($M1$), 611 keV ($M1$), and 1306 keV ($E2$). The multipolarity was assigned using the procedure described earlier. Figure 6 shows a gated spectrum with 350 keV gamma ray as the gate. This gamma ray was known by earlier work to be $E2$ in character. The ordering of the gamma rays was based on the intensity flow argument. The proposed level scheme is shown in Fig. 7.

IV. THEORETICAL DISCUSSION

Spherical shell-model calculations were performed for $N=50$ closed-shell nuclei about two decades ago using ^{88}Sr as the inert core with valence protons occupying the ($2p_{1/2}$, $1g_{9/2}$) configuration space. It is expected that the nuclei lying within this configuration space should be adequately described with ^{88}Sr as the core, since it is known that the $Z=50$ is a j-j coupling closed shell and $Z=40$ is an l-s coupling closed shell. Furthermore, $N=50$ is a well-known closed core. However, in this configuration space, the total maximum angular momentum possible is very limited. For example in the case of ^{93}Tc, the largest angular momentum possible in both the negative and positive parity bands is $J=\frac{25}{2}$.

In the present work high spin states have been established experimentally up to spins of $\frac{39}{2}^+$ and $\frac{43}{2}^-$ for ^{93}Tc. In order to generate such high spin states theoretically in the context of the spherical shell-model scheme, a larger configuration space needs to be employed. Two possible ways exist to generate these high spin states. The first and more obvious way is to employ ^{78}Ni with the valence particle configuration space of ($1f_{5/2}$,$2p_{3/2}$,$2p_{1/2}$,$1g_{9/2}$) as the closed core for which the interaction matrix elements have been recently obtained in Ref. [3]. In this work, the 65 two-body matrix elements and four single particle energies have been obtained in a least-square fit to over 170 energy levels in the nuclei ranging from ^{82}Ge to ^{96}Pd. All details of this fitting procedure may be found in Ref. [3]. Using these interaction matrix elements, we have carried out the spherical shell model calculations using the OXBASH code [12]. The results of these calculations are shown in Fig. 8. It is evident from this figure

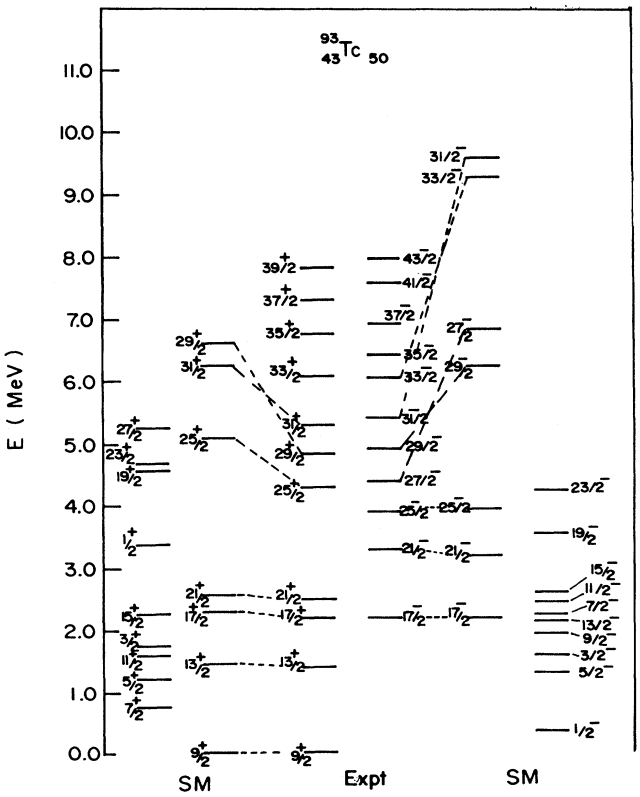

FIG. 8. Comparison of the observed states in ^{93}Tc with spherical shell-model calculations within the ($1f_{5/2}$, $2p_{3/2}$,$2p_{1/2}$,$1g_{9/2}$) model space. Large discrepancies are observed for the states beyond $J=\frac{25}{2}$.

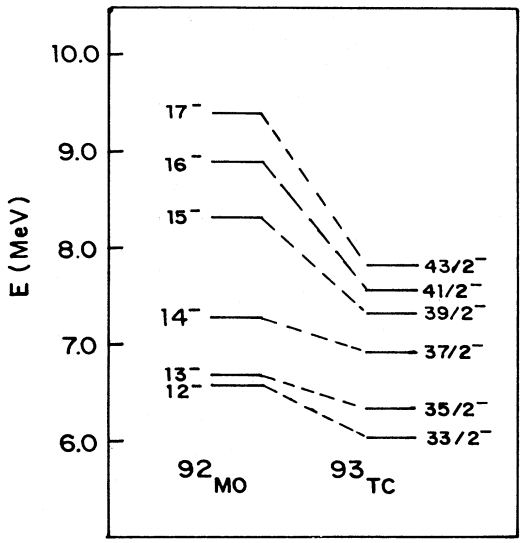

FIG. 9. Comparison of the observed spectra of ^{93}Tc and ^{92}Mo for the negative parity states which correspond to the excitation of a neutron across the shell.

that the states are well reproduced upto a spin of $J=\frac{25}{2}$ in both the positive and negative parity bands. (It is to be noted that the states $\frac{11}{2}^+$, $\frac{15}{2}^+$, and $\frac{19}{2}^+$ lie higher in the excitation energy as compared to the states $\frac{13}{2}^+$, $\frac{17}{2}^+$, and $\frac{21}{2}^+$, respectively, in the shell-model calculations and have not been observed in the present experiment.) Large discrepancies between the observed and the theoretical spectra are seen to exist for higher J states. Hence it appears unlikely that proton excitation is an adequate explanation for the high spin states observed in ^{93}Tc beyond $J=\frac{25}{2}$.

The second approach that one can employ in order to understand the structure of the observed high spin states in ^{93}Tc is the excitation of a neutron from the $N=50$ core to the $2d_{5/2}$ level in the next shell. This kind of analysis has been recently carried out for ^{94}Ru wherein the structure of levels exhibited are in fair agreement with the $N=50$ neutron core excitation calculations. It is also evident from this work that the higher spin states $J=17^+$, 18^+, 19^+ could be adequately represented by the configuration $[^{93}\mathrm{Ru}(J')\otimes\nu d_{5/2}{}^{94}\mathrm{Ru}(J)]$. This weak-coupling approximation scheme as used in ^{94}Ru can be employed to generate high spin states in ^{93}Tc. In the latter case, one could couple a $g_{9/2}$ proton to the ^{92}Mo states which have been recently populated [13] upto $J=17^-$. It has been shown [13] that the high spin levels $J=12^-$, 13^-, 14^-, 15^-, 16^-, and 17^- can be described in a scheme where a neutron is excited from the $(2p_{1/2},1g_{9/2})$ to the $2d_{5/2}$ state in the next shell. A comparison of the spectra for the negative parity band of ^{92}Mo and ^{93}Tc is presented in Fig. 9. It is observed that the spacing of the $J=\frac{33}{2}^-$ to $\frac{43}{2}^-$ states in ^{93}Tc is similar to the $J=12^{-1}$ to 17^- states in ^{92}Mo. The maximum spin one can generate from the coupling of a $g_{9/2}$ proton to ^{92}Mo core is $J=\frac{43}{2}^-$ and this is the highest state observed in ^{93}Tc. More theoretical work, probably using the projected Hartree-Fock approach, needs to be done in order to understand the nature of the intermediate states $J=\frac{29}{2}^-$ to $\frac{31}{2}^-$. It is to be noted that the excitation of the neutron from the $(2p_{1/2},1g_{9/2})$ to the $2d_{5/2}$ state in the next shell, requires a lot of energy which appears as a gap of about 2 MeV in the ^{92}Mo level scheme between the 11^- and 13^- states. In the unperturbed picture this energy gap is approximately $\hbar\omega=7$ MeV. This gap is reduced to 2 MeV in ^{92}Mo due to many-particle correlations. The absence of this large gap in ^{93}Tc is further indicative of the importance of these many-particle correlations. It is worth mentioning that this gap is also absent in ^{94}Ru (Ref. [5]).

Finally, within the shell-model prescription one expects somewhat irregular behavior due to particle excitations. However, it is interesting to note that, the highest three transitions 582, 611, and 529 keV in the positive parity band have almost the same energy.

V. CONCLUSIONS

The level scheme of ^{93}Tc has been substantially extended upto a spin $\frac{39}{2}^+$ in the positive parity band and $\frac{43}{2}^-$ in the negative parity band.

Using ^{88}Sr core with the protons occupying the $(2p_{1/2},1g_{9/2})$ configuration space only low-lying states upto a spin of $\frac{25}{2}$ could be reproduced. The enlargement of the proton configuration space to $(1f_{5/2}, 2p_{3/2},2p_{1/2},1g_{9/2})$ with ^{78}Ni as the closed core does not reproduce the observed spectra above $J=\frac{25}{2}$. Large discrepancies are seen between the calculations and the observed data. The excitation of a neutron from the closed $N=50$ core to the next shell seems to be a possible mechanism for the observation of the high spin states.

The observation of the reduction in the energy gap when a neutron is promoted to the next shell by breaking the $N=50$ core brings to the focus importance of many-particle correlations.

The deformed structures as seen in the $Z=50$ closed-shell nuclei were not observed in the $N=50$ ^{93}Tc nucleus. However, there appears a regularity at the top of the positive parity band which may be an indication of collective behavior. This interesting aspect needs further experimental exploration.

ACKNOWLEDGMENTS

We would like to express our gratitude to Professor A. P. Patro and Professor C. V. K. Baba for many helpful discussions. We are thankful to Professor G. K. Mehta for constant encouragement during the course of the work. Thanks are due to our colleagues Dr. A. M. Narsale, Dr. V. P. Salvi, S. Murlithaar, G. O. Rodrigues, and B. K. Choubisa for their help in the course of the experiment. The help of Pragya Singh in target preparation is gratefully acknowledged. Finally we thank the accelerator staff at the Nuclear Science Centre, New Delhi for their excellent cooperation.

[1] J. D. Ball, J. B. McGrory, and J. S. Larsen, Phys. Lett. **41B**, 581 (1972).
[2] D. H. Gloeckner and F. J. D. Serduke, Nucl. Phys. **A220**, 477 (1974).
[3] Xiandong Ji and B. H. Wildenthal, Phys. Rev. C **37**, 1256 (1988).
[4] Xiandong Ji and B. H. Wildenthal, Phys. Rev. C **38**, 2849 (1988).
[5] K. Muto, T. Shimano, and H. Horie, Phys. Lett. **135B**, 349 (1984).
[6] D. A. Vigars, H. W. Taylor, B. Singh, and J. C. Waddington, Phys. Rev. C **36**, 1006 (1987).
[7] H. Harada, T. Murakami, K. Yoshida, J. Kasagi, T. Inamura, and T. Kubo, Phys. Lett. B **207**, 17 (1988).
[8] H. Harada, M. Sugawara, H. Kusakari, H. Shinohara, Y. Ono, K. Furuno, T. Hosoda, M. Adachi, S. Matsuki, and N. Kawamura, Phys. Rev. C **39**, 132 (1989).
[9] B. A. Brown, D. B. Fossan, P. M. S. Lesser, and A. R. Poletti, Phys. Rev. C **13**, 1194 (1976).
[10] M. Grecescu, A. Nilsson, and L. Harms-Ringdahl, Nucl. Phys. **A212**, 429 (1973).
[11] F. S. Stephens, M. A. Deleplanque, R. M. Diamond, A. O. Macchiavelli, and J. E. Draper, Phys. Rev. Lett. **54**, 2584 (1985).
[12] B. A. Brown and B. H. Wildenthal, Annu. Rev. Nucl. Part. Sci. **38**, 29 (1988).
[13] P. Singh, R. G. Pillay, J. A. Sheikh, and H. G. Devare, Phys. Rev. C **45**, 2161 (1992).